Magnetic, Antiferroelectric Like Behavior, and Resistance Switching Properties in $BiFeO_3$-$CaMnO_3$ Polycrystalline Thin Films

Abdelilah LAHMAR *, Jacem Zidani, Jamal Belhadi, Ilham Hamdi Alaoui, Hussam Musleh, Jihad Asaad, Naji Al Dahoudi, Mimoun El Marssi

Posted Date: 17 October 2023

doi: 10.20944/preprints202310.1038.v1

Keywords: ferromagnetic; Antiferroelectric like; polycrystalline films, BiFeO3-CaMnO3; Resistance switching

Article

Magnetic, Antiferroelectric Like Behavior, and Resistance Switching Properties in $BiFeO_3$-$CaMnO_3$ Polycrystalline Thin Films

Abdelilah Lahmar [1,*], Jacem Zidani [1], Jamal Belhadi [1], Ilham Hamdi Alaoui [1], Hussam Musleh [2], Jehad Asad [2], Naji Al Dahoudi [2] and Mimoun El Marssi [1]

[1] Condensed Matter Physics Laboratory (LPMC), University of Picardie Jules Verne, 33 Rue Saint Leu, 80000 Amines, France

[2] Al Azhar University-Gaza, Physics Department, P.O. Box 1277, Gaza, Palestine

* Correspondence: abdel.ilah.lahmar@u-picardie.fr; Tel.: +33-3-22-82-76-91

Abstract: The effect of ferromagnetic $CaMnO_3$ (CMO) addition on structural, magnetic, dielectric, and ferroelectric properties of $BiFeO_3$ are presented. X ray diffraction and Raman investigation allowed the identification of single pseudo cubic perovskite structure. The magnetic measurement showed that the prepared films exhibit a ferromagnetic behavior at low temperature with both coercive field and remnant magnetization increased with increasing CMO content. However, a deterioration of magnetization was observed at room temperature. Ferroelectric study revealed an antiferroelectric like behavior with a pinched P-E hysteresis loop for 5%CMO doping BFO resulting in low remnant polarization and double hysteresis loops. Whereas, high remnant polarization and coercive field with a likely square hysteresis loop are obtained for 10 % CMO addition. Furthermore, a bipolar resistive switching behavior with a threshold voltage of about 1.8V is observed for high doped film that can be linked to the ferroelectric polarization switching.

Keywords: ferromagnetic; antiferroelectric like; polycrystalline films, $BiFeO_3$-$CaMnO_3$; resistance switching

1. Introduction

Interest in multiferroic materials has been steadily growing due to their interlinked electric, magnetic, and structural order parameters, resulting in concurrent ferromagnetic, ferroelectric, and magnetoelectric characteristics [1–3]. Among these materials, $BiFeO_3$ (BFO), which has been extensively investigated, exhibits ferroelectric behavior with a Curie temperature (TC) of 1083 K and G-type antiferromagnetic properties with a (TN) of 643 K [4,5]. Furthermore, it maintains a distorted rhombohedral structure within the (R3c) space group at room temperature, rendering it an appealing option for numerous technological applications [6,7]. A review of the literature has revealed that bulk BFO is susceptible to high leakage currents attributed to defects within its matrix [8,9]. However, BFO thin films have garnered increased attention due to reported enhancements in remnant polarization (*Pr*) and magnetization when compared to bulk single crystal [10]. Nevertheless, the low resistivity of BFO films can impede polarization switching, representing a significant concern primarily due to the complex defect chemistry [11–13]. It is important to note that reducing the grain size and appropriate doping can effectively mitigate leakage currents in BFO, improving its microstructure. Extensive research has been conducted to enhance the electrical and magnetic properties of BFO through doping strategies [8,14–22].

It is worth noting that significant progress has been made in showcasing the multifunctionality of BFO-based materials. Notably, researchers have reported intriguing enhancements in multiferroic properties in both epitaxial and polycrystalline BFO-based thin films. For instance, the incorporation of rare-earth elements into epitaxial BFO thin films has led to the emergence of a morphotropic phase boundary (MPB) between the rhombohedral phase (*R3c*) and orthorhombic phase (*Pnma*) at a critical composition of x=0.14, particularly for elements such as Gd and Sm. In this composition range, distinctive features such as pinched hysteresis loops with small remnant polarization have been documented, indicating the presence of an antiferroelectric-like behavior in these compositions

 doi:10.20944/preprints202310.1038.v1

[23,24]. Transmission electron microscopy investigations have provided corroborating evidence of local ordering, similar to what is observed in antiferroelectric (AFE) $PbZrO_3$ materials [25]. The observation of this region holds particular promise for achieving a significant piezoelectric response. However, it is important to note that the macroscopic response of these compositions continues to exhibit primarily ferroelectric behavior.

On the other hand, the phenomenon of resistance switching (RS) in BFO-based materials has garnered significant attention, particularly in the context of non-volatile memory devices. Y. Shuai et al. reported a nonvolatile bipolar resistive switching in Au/$BiFeO_3$/Pt configurations [26]. Additionally, Xinman Chen et al. documented bipolar RS behaviors in $BiFeO_3$ thin films with Pt/$BiFeO_3$/LNO setups [27]. The strategy of doping BFO has also emerged as a compelling avenue for enhancing RS properties. Yang C. H et al. observed such properties in Ca-doped BiFeO3 films, employing conductive atomic force microscopy [28]. Furthermore, Mi Li et al. reported RS behavior in metal/$Bi_{0.95}La_{0.05}FeO_3$/Pt sandwiched structures [29]. Through this brief literature review, it becomes evident that BFO-based materials continue to captivate researchers in the field of multiferroics due to their adaptability and multifunctionality. Notably, their physical and chemical properties can be readily adjusted to achieve desired characteristics.

Prior studies have demonstrated that the incorporation of $RMnO_3$ (where R represents a rare-earth element) into BFO thin films can effectively enhance both ferroelectric and magnetic properties, even at doping concentrations of up to 10% [30]. These investigations have revealed that even a minor doping concentration can instigate significant structural changes, characterized by the emergence of Jahn-Teller distortion. This structural transformation has been ascribed to the presence of Mn^{3+} ions within the BFO matrix [31]. However, it is noteworthy that the substitution of Bi^{3+} ions, which are stereochemically active lone pair ions, with lanthanide elements, which are nonstereochemically active ions, appears to lead to a reduction in the stereochemical activity of Bi–O bonds.

In pursuit of exploring additional functionalities and advancing our research on the impact of manganates on the physico-chemical properties of BFO polycrystalline films, our present study focuses on the influence of the manganite compound $CaMnO_3$. In our previous research, we extensively discussed the presence of Mn^{3+} ions occupying Fe^{3+} sites, demonstrating its critical role in maintaining polarization switching behavior [30,31]. Conversely, the incorporation of Ca^{2+} ions into the Bi^{3+} sites has been noted as particularly intriguing for inducing resistance switching behavior [32–34]. Additionally, Lu Liu et al. reported the coexistence of unipolar and bipolar resistive switching in $Bi_{0.8}Ca_{0.2}FeO_3$ polycrystalline thin films [32]. In this work, we place emphasis on the fabrication of $BiFeO_3$-x$CaMnO_3$ polycrystalline thin films and the comprehensive investigation of their structural, magnetic, and electrical properties. Remarkably, our findings reveal the presence of an antiferroelectric-like characteristic within our system, coexisting with resistance switching behavior. This discovery holds significant promise for distinguishing between ferroresistive effects [9] and charge-trapping phenomena [35].

2. Materials and Methods

Thin films were synthesized through a spin-coating process onto a commercial (111)-Pt/Ti/SiO_2/Si substrate heterostructure. The initial materials used were Bi-acetates and Gd acetates tetrahydrate (sourced from Alpha easer, Germany), as well as Mn, Fe, Co, and Cr acetylacetonate (obtained from Sigma-Aldrich, Germany). These compounds were dissolved in a mixture of propionic acid and 2-methoxyethanol in a volume ratio of 1:2, resulting in a sol concentration of 0.22 mol/l. Pyrolysis of the sol-gel was carried out on a hot plate set at 260 °C. Subsequently, a final annealing process was conducted within a preheated tube furnace under a saturated oxygen atmosphere at 650 °C for a duration of 60 minutes. The thickness of the resulting films after annealing was determined using scanning electron microscopy (SEM) on cross-sections. Microstructural analysis of the prepared samples was performed using a SEM Philips XL30 device operating at 5kV. The thin films obtained in this study underwent several characterization techniques. Firstly, X-ray diffraction analysis was carried out at room temperature using a four-circle high-resolution D8 Discover Bruker diffractometer equipped with a Göbel mirror. Cu Kα radiation with a wavelength

Preprints (www.preprints.org) | NOT PEER-REVIEWED | Posted: 17 October 2023 doi:10.20944/preprints202310.1038.v1

(ƛ) of 1.5418 Å was utilized for this analysis. Additionally, Raman spectroscopy was performed in a back-scattering configuration using a micro-Raman Renishaw spectrometer, with a green laser excitation source emitting at 514.5 nm. The laser power was carefully maintained below 20 mW to prevent any sample heating effects. For the assessment of magnetic properties, a commercial Physical Property Measurement System (PPMS DynaCool, Quantum Design) was employed. Magnetization measurements ($M(T)$) were conducted at both 2 K and 300 K, with an applied magnetic field up to H = 1 kOe. Dielectric measurements were carried out as a function of temperature and over a frequency range spanning from 100 Hz to 1 MHz. These measurements were performed using a Solartron Impedance analyzer SI-12060, with a probing AC electric field amplitude of 100 mV. Ferroelectric investigations were conducted by measuring the polarization–electric field (P-E) hysteresis loops at a frequency of 10 kHz. A TF Analyzer 3000, aix-ACCT system, was employed for this purpose. To assess the leakage current properties, a Keithley 2611 A source was utilized. All electrical measurements were executed using a metal–dielectric–metal geometry, with sputtered-Pt circular top electrodes featuring diameters of 250 μm. These electrodes were deposited through a shadow mask to ensure precise placement.

3. Results

3.1. Microstructural and Structural investigation

Figure 1(a) and (b) present the scanning electron microscopy (SEM) images of the prepared thin films. In the case of the 5CaBFOM phase, the microstructure reveals plate-like grains, with distinct grain boundaries that are readily visible. It's worth noting that as the concentration of doping elements increases, it results in the fragmentation of larger grains, leading to a noticeable reduction in grain size. The average grain sizes were measured to be 130 nm and 89 nm for the 5CaBFOM and 10CaBFOM thin films, respectively. it seems that the increasing of the CMO concentration inhibits the grain growth while sintering.

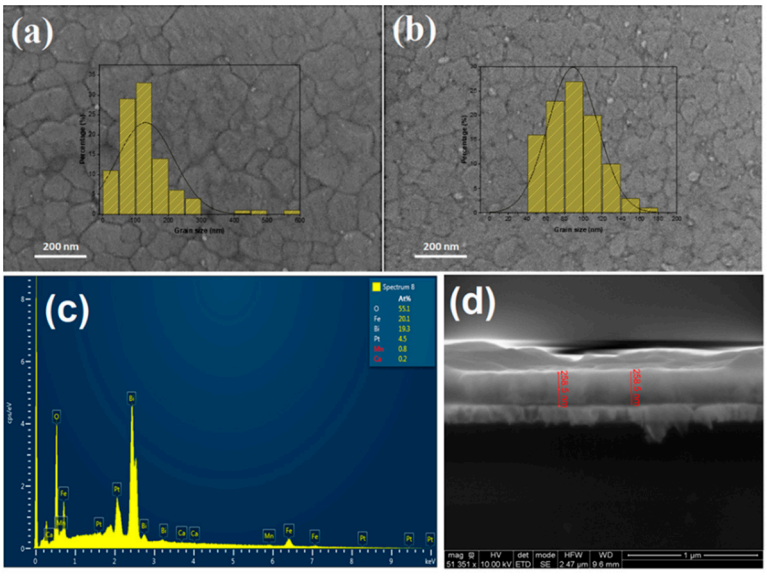

Figure 1. Surface morphologies of studied specimens: (a) 5CaBFOM; (b) 10CaBFOM, (c) example on EDX analysis for 10CaBFOM film, (d) example of cross section for 10CaBFOM film.

The EDX spectra carried out on both films showed the expected starting elements Bi, Fe, Ca, Mn, and O. Figure 1 (c) shows an example of the EDX analysis carried out on10CaBFOM film. The average thickness of the prepared films was found to be approximately 280 nm (see Fig.1(d) as example). Figure 2 illustrates the X-ray diffraction (XRD) patterns of the films under investigation, with the reflections indexed based on a pseudocubic unit cell. Both films exhibited pure perovskite phases, and these findings are considered accurate within the precision of the employed device. It is indeed

Preprints (www.preprints.org) | NOT PEER-REVIEWED | Posted: 17 October 2023 doi:10.20944/preprints202310.1038.v1

challenging to discern detailed structural changes when transitioning from a 5% to a 10% $CaMnO_3$ concentration. Nevertheless, a noticeable trend emerges in favor of orientation in the (h00) direction when comparing the diffraction patterns. Remarkably, the splitting reflections (110) and (−110), which are observed in pure BFO [9], were not detected upon doping with $CaMnO_3$. Instead, they appear to have merged into a single peak around 32° (2θ), consistent with previous reports that have linked this phenomenon to structural transformations [30,31]. Additionally, upon closer examination of the position of the (100) reflection (as depicted in the inset), a clear shift towards higher angles is evident with an increase in the $CaMnO_3$ concentration to 10%. The lattice spacing, determined from the (100) pseudocubic peaks (d_{100} values), closely approximates the in-plane lattice spacing of Pt (100), which is 0.3923 nm. This alignment suggests a good lattice match between the prepared thin films and the Pt-crystal substrate as a possible contributing factor to these observations.

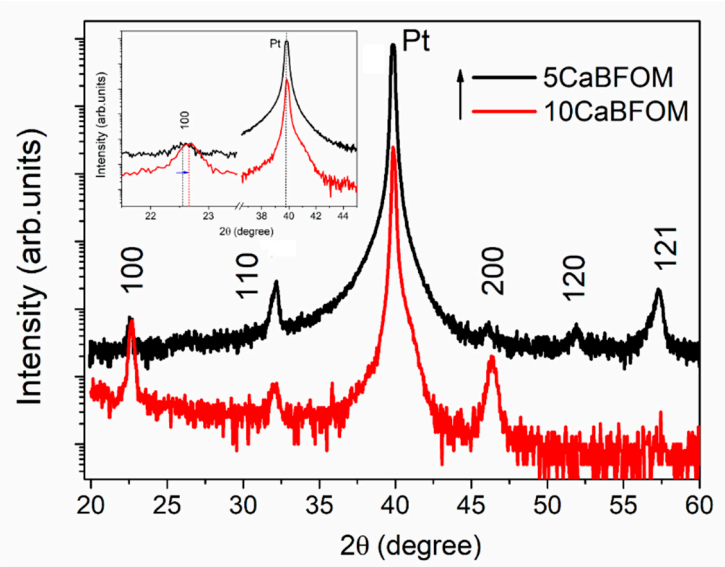

Figure 2. XRD pattern of (a) 5CaBFOM, (b) 10CaBFOM deposited on (111)-Pt/Ti/SiO2/Si, Pt denotes peaks belonging to the substrate. The reflections are indexed according to a pseudocubic unit cell.

Raman spectroscopy was employed to gain further structural insights not accessible through X-ray diffraction (XRD). Figure 3 displays the Raman spectra of both studied films. As evident from the figure, all vibration modes observed at frequencies below 300 cm^{-1} can be attributed to Bi–O covalent bonds. Additionally, two broad bands appear around 620 cm^{-1} and within the range of 450 to 550 cm^{-1}, corresponding to symmetric and antisymmetric stretching modes, respectively. In comparison to pure $BiFeO_3$ (the parent phase) [36], the presence of these bands is associated with the basal oxygen ions of the $Mn^{3+}O_6$ octahedra, which are linked to Jahn–Teller (JT) distortion. Further discussion regarding the development of these features when doping BFO with rare earth manganite can be found in our prior research [37]. It's worth noting that in the present study, there is no discernible change in the Raman spectrum when the concentration is increased from 5% to 10% $CaMnO_3$ doping. However, it is interesting to mention that the band attributed to JT distortion in this work is not as pronounced as in the case of $RMnO_3$ modified BFO, possibly due to the presence of Mn^{4+} ions, which may contribute to a reduction in the JT distortion (as discussed in the magnetic analysis).

Preprints (www.preprints.org) | NOT PEER-REVIEWED | Posted: 17 October 2023 doi:10.20944/preprints202310.1038.v1

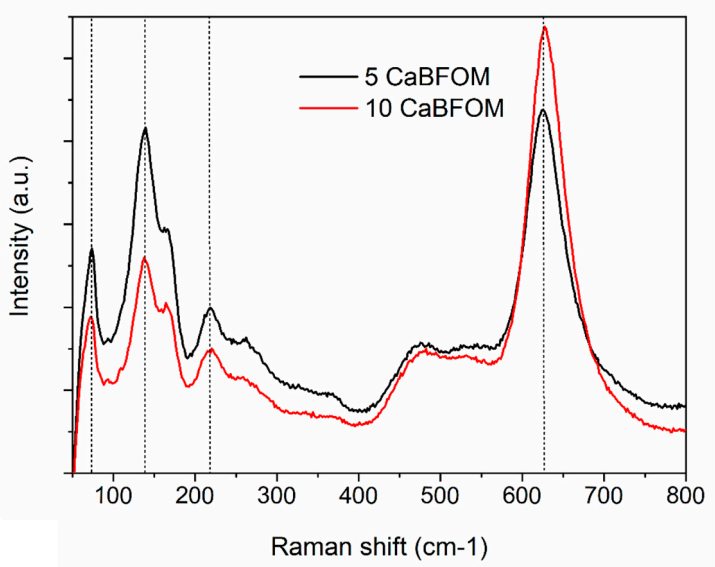

Figure 3. Raman spectra of the investigated specimens

3.2. Magnetic investigations

The magnetic hysteresis curves for the studied specimens at both room temperature (RT) and 2K are presented in Figure 4. It's worth noting that $CaMnO_3$ is recognized as an antiferromagnetic insulator (AFMI) material, characterized by the presence of both four- and tri-valent manganese ions [38]. This manganite exhibits a complex magnetic behavior at low temperatures, transitioning from antiferromagnetic (G-type AFM) to paramagnetic ordering with a Neel temperature around 125 K, and eventually revealing a weak ferromagnetic component below 10 K [39–41].

The strong G-type antiferromagnetic (AFM) order observed at 120–125 K in $CaMnO_3$ is attributed to superexchange interactions between Mn^{3+} and Mn^{4+} ions. Conversely, the ferromagnetic (FM) order in CMO arises from the presence of double exchange interactions [42,43]. In the present study, as depicted in Figure 4(a), there is no significant improvement in magnetization observed at room temperature when compared to what is observed for the BFO thin film. However, a decrease in magnetic properties is evident when increasing the CMO content from 5% to 10% at room temperature. Similar behavior was reported with the addition of $LaMn_{0.5}Co_{0.5}O_3$ to BFO thin films [44]. Interestingly, the influence of CMO addition on magnetization becomes more pronounced at low temperatures. As shown in Figure 4(b), clear ferromagnetic hysteresis is observed for both investigated films. Notably, the increase in CMO content results in an elevation of the magnetic coercive field, indicating that the material becomes magnetically hard. This behavior is plausible when considering that the increase in CMO content leads to a corresponding increase in magnetic interactions.

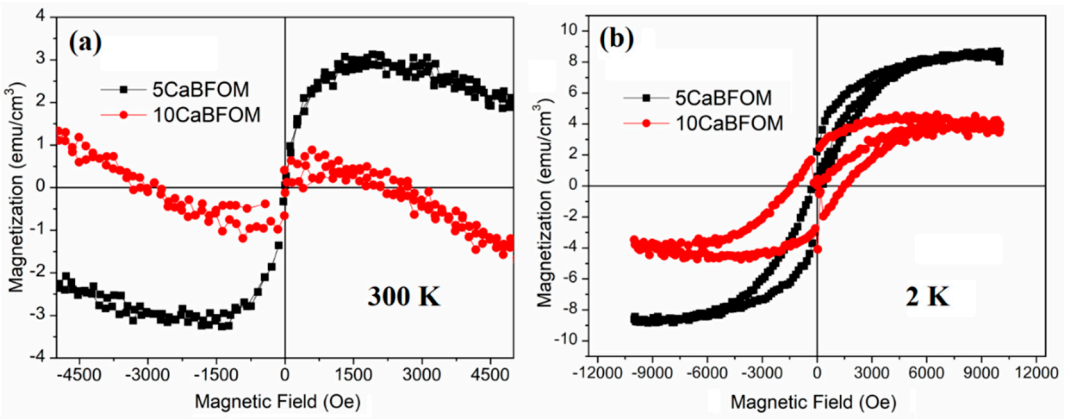

Figure 4. Magnetic hysteresis loop for the investigated thin films: (a) at 2K; (b) at 300K.

Preprints (www.preprints.org) | NOT PEER-REVIEWED | Posted: 17 October 2023 doi:10.20944/preprints202310.1038.v1

3.3. Dielectric and ferroelectric investigation

In order to investigate the impact of $CaMnO_3$ doping on the dielectric and ferroelectric properties of $BiFeO_3$, we conducted measurements of dielectric permittivity and polarization on both of the studied samples.

In Figure 5, we present the dielectric permittivity and losses as functions of frequency at room temperature for both the 5CaBFMO and 10CaBFMO samples. Initially, it is evident that both samples exhibit a consistent decrease in the dielectric constant as the frequency increases. Concurrently, the dielectric losses are notably higher at lower frequencies but decrease significantly as the frequency rises, reaching minimum values of 0.05 and 0.06, respectively. These findings are indicative of space charge activation at lower frequencies, a well-known phenomenon in BFO-based materials.

Furthermore, it is worth noting the observed increase in dielectric losses between 10^5 and 10^6 Hz, which is attributed to the phenomenon of dielectric relaxation. In fact, the charge carriers in the films cannot follow the external electric field, resulting in the maximum electrical energy being transferred to the oscillation ions [45]. Secondly, we observe that the dielectric permittivity of the 5CaBFMO sample is approximately two times higher than that of the 10CaBFMO sample. This difference can be attributed to domain pinning resulting from the presence of dipole defects (further discussed below).

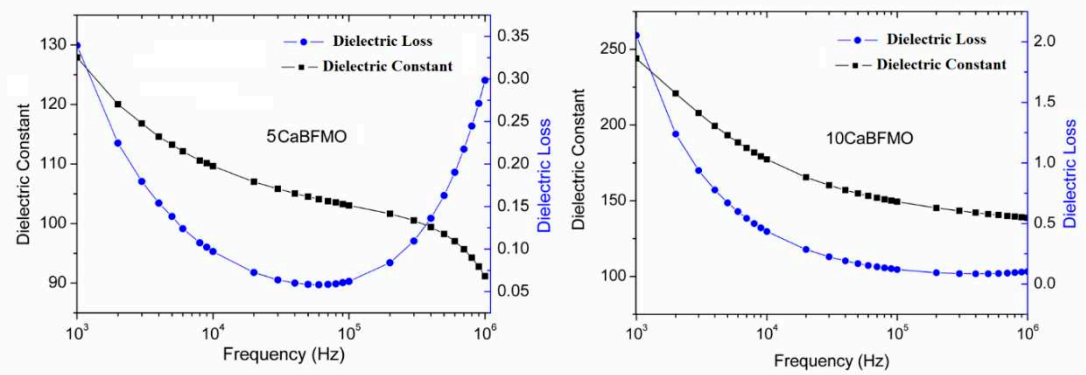

Figure 5. *Magnetic hysteresis loop for the investigated thin films: (a) at 2K; (b) at 300K.*

Figure 6 (a and c) showcase the ferroelectric *P-E* hysteresis loops measured at room temperature for the 5CaBFMO and 10CaBFMO films at various frequencies. In both cases, the films exhibit fully saturated P-E loops with a remarkably high maximum polarization exceeding 40 $\mu C/cm^2$. It's important to note that we observe an enhancement in maximum polarization as the frequency decreases. This increase can be attributed to the impact of leakage currents, which become more prominent at lower frequencies, as evidenced in the dielectric measurements. Another noteworthy observation is that 5CaBFMO film exhibits a clear double *P-E* loop. Figure 6 (b and d) depict the *P-E* loops and their corresponding polarization current switching measured at 10 kHz for the 5CaBFMO and 10CaBFMO films, respectively. The polarization current curves for both films reveal the presence of four switching current peaks, a characteristic indicative of AFE or non-ergodic states. The observed AFE character can be attributed to the formation of various defect dipoles involving oxygen and cation vacancies, aimed at achieving charge balance within the material. In ferroelectrics, ordered defect dipoles can act as pinning centres within domains, impeding the switching of ferroelectric domains when exposed to an externally applied electric field [46,47]. It's worth noting that the electric field corresponding to the current peak I_1, which signifies the transition from antiferroelectric-like to ferroelectric behavior (EAFE-FE), is twice as high in the 5CaBFMO film compared to the 10CaBFMO film. This observation implies that the static electric field generated by dipole defects is stronger in the 5CaBFMO film. This higher internal static electric field can hinder long-range polar order, resulting in a lower remanent polarization with clear antiferroelectric (AFE)-like

Preprints (www.preprints.org) | NOT PEER-REVIEWED | Posted: 17 October 2023 doi:10.20944/preprints202310.1038.v1

behavior observed in the 5CaBFMO film. This phenomenon can explain the lower dielectric permittivity observed in the 5CaBFMO film due to increased domain pinning.

In tier theoretical work, Bin Xu et al. [48] reported that the pinched loop is probable when FE and EFE are very close to each other in energy at morphotropic phase boundaries (MPB). The authors surmise that this type of behavior occurs in the so-called hybrid improper ferroelectrics where a larger anti-polar amplitude and a small finite polarization exist simultaneously.

It's important to mention that the generation of a double hysteresis loop in ferroelectric $BiFeO_3$ materials has potential applications in innovative nanodevices, including high-density multistate data storage [46]. This property opens up opportunities for exploiting the unique characteristics of these materials in advanced technological applications.

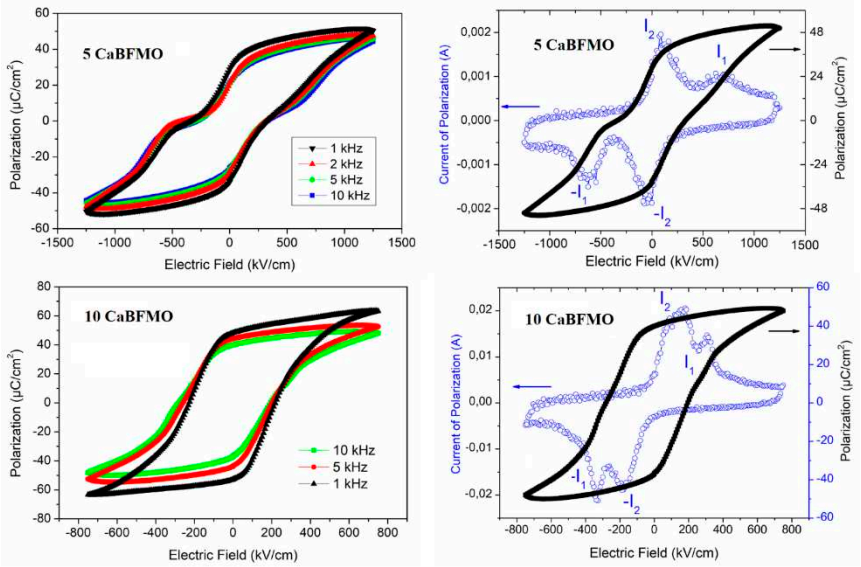

Figure 6. Room temperature Polarization hysteresis P-E loops at different frequencies for (a) 5CaBFMO and (c) 10CaBFMO thin films. (b) and (c) show the P-E loops and the corresponding polarization current switching at 10kHz of 5CaBFMO and 10CaBFMO, respectively.

3.4. Resisting switching behavior

Electrical measurements have revealed that all of our samples exhibit resistive switching behavior without the need for any forming process. Figure 7 displays the current-bias (IV) curve for Pt/CaBFMO/Pt films, with a maximum applied voltage of 5V. The obtained IV curves are nearly symmetric. In the case of Pt/5CaBFMO/Pt, shown in Figure 7(a), a weak hysteresis is observed in the positive voltage polarity. It's important to note that this film exhibits antiferroelectric-like behavior, typically attributed to an internal bias field established by defect dipoles. These results suggest that charge carriers localized near interfaces do not contribute significantly to the resistive switching. It is known that Mn doping can significantly reduce leakage current in BFO films and enhance ferroelectric polarization. Several studies have demonstrated that ferroelectric polarization charges can control resistive switching in BFO thin films [49]. In this case, the 5% CMO content incorporated into the BFO matrix does not result in a fully saturated ferroelectric hysteresis loop and does not induce resistive switching either. Therefore, it appears that no charges-trapping effect is prominent in this film.

However, in the case of the Pt/10CaBFMO/Pt film (Figure 7(b)), where the CMO concentration is 10%, the scenario is different.

Preprints (www.preprints.org) | NOT PEER-REVIEWED | Posted: 17 October 2023 doi:10.20944/preprints202310.1038.v1

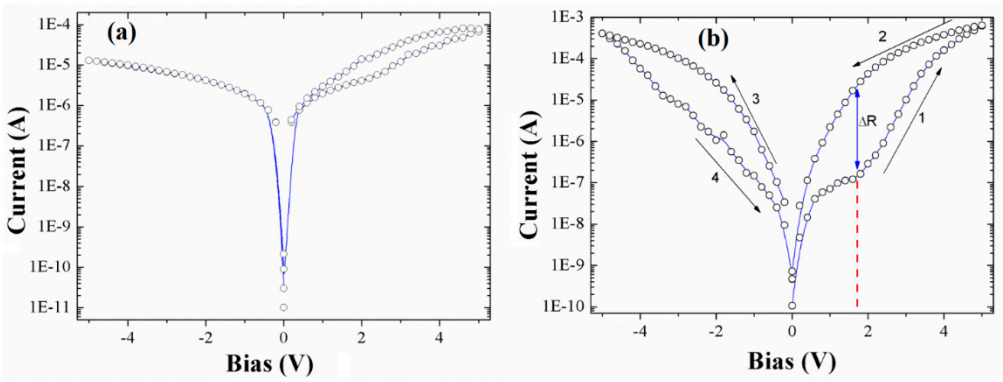

Figure 7. IV characteristics of: (a) 5Ca BFMO thin film. (b) 10Ca BFMO thin film. Noting that the positive voltage is applied to the Pt top electrode.

In the case of the Pt/10CaBFMO/Pt film, the resistive switching behavior is notable. Initially, the BFO film is in a high-resistance state, and at around 1.8V, the film switches to a low-resistance state. Interestingly, the 10CaBFMO film can be switched back to a high-resistance state by applying a negative voltage (< -1.8V). The resistance ratio (ΔR) obtained for the positive bias region, as indicated by the blue arrow, demonstrates a change of approximately 3 orders of magnitude. The resistance ratio deduced from this figure is roughly 10^3, which is a high value comparable to that reported in similar systems [50]. This high value positions our film as a promising candidate for non-volatile resistive memories, as a resistance ratio of 10 is typically considered competitive with Flash technology [51,52].

It's important to note that this bipolar resistive switching, with a threshold voltage (the set tension) of about 1.8V (indicated by the red dashed line in Figure 7(b)), can be directly related to the ferroelectric polarization observed in this film. However, it's worth mentioning that the current hysteresis in our case is not perfectly anti-symmetric. In fact, the resistance ratio obtained in the negative bias region is smaller. This suggests that interfaces play a relatively smaller role in resistance switching compared to the impact of ferroelectric polarization in our system.

4. Conclusions

In summary, the addition of $CaMnO_3$ had significant effects on the structural, magnetic, and electrical properties of BFO thin films. Magnetic investigations revealed that the magnetic characteristics of BFO were strongly influenced by $CaMnO_3$, resulting in a ferromagnetic order at low temperatures and an antiferromagnetic order at room temperature. In the ferroelectric study, the 5CaBFMO film displayed a pinched hysteresis loop, while the 10CaBFMO film exhibited a well-saturated loop. Intriguingly, the polarization current curves for both films displayed the presence of four switching current peaks, characteristic of antiferroelectric-like behavior. It appears that the co-doping of Ca and Mn into the BFO matrix induced changes in the cation ordering at the A/B-sites, leading to local structural heterogeneity that varied with the concentration of $CaMnO_3$. Additionally, reversible resistive switching was observed in the 10CaBFMO film when an electric field was applied. Overall, the co-doping of BFO with Ca and Mn ($CaMnO_3$) shows promise for enhancing the functionalities of BFO materials, opening up opportunities for advanced applications and novel device technologies.

Author Contributions: Conceptualization, A.L.; validation, M.E, B.J and N.AD; formal analysis, I.A, J.Z., J.A; investigation, A.L, J.Z., I.A, H.M; data curation, H.M., J.B., J.A; writing—original draft preparation, A.L.; writing—review and editing, L.A., M.E, J.B, N.AD; All authors have read and agreed to the published version of the manuscript.

Funding: Financial support of this work was provided by the PHC AL MAQDISI 2021 grant No. 48024ZF.

Data Availability Statement: Not applicable.

Acknowledgments: Dr. Hussam Musleh would like to thank the "Ambassade de France à Jérusalem" for Scientific High-Level Visiting Fellowships (SSHN) 2023.

Conflicts of Interest: The authors declare no conflict of interest results.

References

1. M.I. Bichurin, Short introduction to the proceedings of the 3 RD international conference on magnetoelectric interaction phenomena in crystals, MEIPIC-3, Ferroelectrics. 204 (1997) xvii–xx. https://doi.org/10.1080/00150199708222180.
2. H. Schmid, Introduction to the proceedings of the 2nd international conference on magnetoelectric interaction phenomena in crystals, MEIPIC-2, Ferroelectrics. 161 (1994) 1–28. https://doi.org/10.1080/00150199408213348.
3. W. Eerenstein, N.D. Mathur, J.F. Scott, Multiferroic and magnetoelectric materials, Nature. 442 (2006) 759–765. https://doi.org/10.1038/nature05023.
4. R.T. Smith, G.D. Achenbach, R. Gerson, W.J. James, Dielectric Properties of Solid Solutions of BiFeO3 with Pb(Ti, Zr)O3 at High Temperature and High Frequency, J. Appl. Phys. 39 (1968) 70–74. https://doi.org/10.1063/1.1655783.
5. J.M. Moreau, C. Michel, R. Gerson, W.J. James, Ferroelectric BiFeO3 X-ray and neutron diffraction study, J. Phys. Chem. Solids. 32 (1971) 1315–1320. https://doi.org/10.1016/S0022-3697(71)80189-0.
6. T. Lottermoser, T. Lonkai, U. Amann, D. Hohlwein, J. Ihringer, M. Fiebig, Magnetic phase control by an electric field, Nature. 430 (2004) 541–544. https://doi.org/10.1038/nature02728.
7. D. Sando, A. Barthélémy, M. Bibes, BiFeO3 epitaxial thin films and devices: past, present and future, J. Phys. Condens. Matter. 26 (2014) 473201. https://doi.org/10.1088/0953-8984/26/47/473201.
8. Y. Wang, C.-W. Nan, Enhanced ferroelectricity in Ti-doped multiferroic BiFeO3 thin films, Appl. Phys. Lett. 89 (2006) 052903. https://doi.org/10.1063/1.2222242.
9. A. Lahmar, K. Zhao, S. Habouti, M. Dietze, C.-H. Solterbeck, M. Es-Souni, Off-stoichiometry effects on BiFeO3 thin films, Solid State Ion. 202 (2011) 1–5. https://doi.org/10.1016/j.ssi.2011.03.017.
10. J. Wang, J.B. Neaton, H. Zheng, V. Nagarajan, S.B. Ogale, B. Liu, D. Viehland, V. Vaithyanathan, D.G. Schlom, U.V. Waghmare, N.A. Spaldin, K.M. Rabe, M. Wuttig, R. Ramesh, Epitaxial BiFeO3 Multiferroic Thin Film Heterostructures, Science. 299 (2003) 1719–1722. https://doi.org/10.1126/science.1080615.
11. X. Qi, J. Dho, M. Blamire, Q. Jia, J.-S. Lee, S. Foltyn, J.L. MacManus-Driscoll, Epitaxial growth of BiFeO3 thin films by LPE and sol–gel methods, J. Magn. Magn. Mater. 283 (2004) 415–421. https://doi.org/10.1016/j.jmmm.2004.06.014.
12. Z. Liu, H. Liu, G. Du, J. Zhang, K. Yao, Electric properties of BiFeO3 films deposited on LaNiO3 by sol-gel process, J. Appl. Phys. 100 (2006) 044110. https://doi.org/10.1063/1.2335399.
13. W. Eerenstein, F.D. Morrison, F. Sher, J.L. Prieto, J.P. Attfield, J.F. Scott, N.D. Mathur, Experimental difficulties and artefacts in multiferroic and magnetoelectric thin films of BiFeO3, Bi 0.6 Tb 0.3 La 0.1 FeO3 and BiMnO3, Philos. Mag. Lett. 87 (2007) 249–257. https://doi.org/10.1080/09500830601173053.
14. H. Liu, Z. Liu, X. Li, X. Li, K. Yao, Bi 1− x La x FeO3 films on LaNiO3 bottom electrode by the sol–gel process, J. Phys. Appl. Phys. 40 (2007) 242–246. https://doi.org/10.1088/0022-3727/40/1/021.
15. S.K. Singh, H. Ishiwara, K. Maruyama, Room temperature ferroelectric properties of Mn-substituted BiFeO3 thin films deposited on Pt electrodes using chemical solution deposition, Appl. Phys. Lett. 88 (2006) 262908. https://doi.org/10.1063/1.2218819.
16. S.R. Shannigrahi, A. Huang, D. Tripathy, A.O. Adeyeye, Effect of Sc substitution on the structure, electrical, and magnetic properties of multiferroic BiFeO3 thin films grown by a sol–gel process, J. Magn. Magn. Mater. 320 (2008) 2215–2220. https://doi.org/10.1016/j.jmmm.2008.04.119.
17. H. Uchida, R. Ueno, H. Funakubo, S. Koda, Crystal structure and ferroelectric properties of rare-earth substituted BiFeO3 thin films, J. Appl. Phys. 100 (2006) 014106. https://doi.org/10.1063/1.2210167.
18. G.L. Yuan, S.W. Or, Multiferroicity in polarized single-phase Bi0.875Sm0.125FeO3 ceramics, J. Appl. Phys. 100 (2006) 024109. https://doi.org/10.1063/1.2220642.
19. M. Azuma, H. Kanda, A.A. Belik, Y. Shimakawa, M. Takano, Magnetic and structural properties of BiFe1−xMnxO3, J. Magn. Magn. Mater. 310 (2007) 1177–1179. https://doi.org/10.1016/j.jmmm.2006.10.287.
20. C.-F. Chung, J.-P. Lin, J.-M. Wu, Influence of Mn and Nb dopants on electric properties of chemical-solution-deposited BiFeO3 films, Appl. Phys. Lett. 88 (2006) 242909. https://doi.org/10.1063/1.2214138.
21. C. Fanggao, S. Guilin, F. Kun, Q. Ping, Z. Qijun, Effect of Gadolinium Substitution on Dielectric Properties of Bismuth Ferrite, J. Rare Earths. 24 (2006) 273–276. https://doi.org/10.1016/S1002-0721(07)60379-2.
22. J.K. Kim, S.S. Kim, W.-J. Kim, A.S. Bhalla, R. Guo, Enhanced ferroelectric properties of Cr-doped BiFeO3 thin films grown by chemical solution deposition, Appl. Phys. Lett. 88 (2006) 132901. https://doi.org/10.1063/1.2189453.
23. D. Kan, L. Pálová, V. Anbusathaiah, C.J. Cheng, S. Fujino, V. Nagarajan, K.M. Rabe, I. Takeuchi, Universal Behavior and Electric-Field-Induced Structural Transition in Rare-Earth-Substituted BiFeO3, Adv. Funct. Mater. 20 (2010) 1108–1115. https://doi.org/10.1002/adfm.200902017.

24. D. Kan, C.-J. Cheng, V. Nagarajan, I. Takeuchi, Composition and temperature-induced structural evolution in La, Sm, and Dy substituted BiFeO3 epitaxial thin films at morphotropic phase boundaries, J. Appl. Phys. 110 (2011) 014106. https://doi.org/10.1063/1.3605492.
25. C.-J. Cheng, D. Kan, S.-H. Lim, W.R. McKenzie, P.R. Munroe, L.G. Salamanca-Riba, R.L. Withers, I. Takeuchi, V. Nagarajan, Structural transitions and complex domain structures across a ferroelectric-to-antiferroelectric phase boundary in epitaxial Sm-doped BiFeO3 thin films, Phys. Rev. B. 80 (2009) 014109. https://doi.org/10.1103/PhysRevB.80.014109.
26. Y. Shuai, S. Zhou, D. Bürger, M. Helm, H. Schmidt, Nonvolatile bipolar resistive switching in Au/BiFeO3/Pt, J. Appl. Phys. 109 (2011) 124117. https://doi.org/10.1063/1.3601113.
27. X. Chen, H. Zhang, K. Ruan, W. Shi, Annealing effect on the bipolar resistive switching behaviors of BiFeO3 thin films on LaNiO3-buffered Si substrates, J. Alloys Compd. 529 (2012) 108–112. https://doi.org/10.1016/j.jallcom.2012.03.014.
28. C.-H. Yang, J. Seidel, S.Y. Kim, P.B. Rossen, P. Yu, M. Gajek, Y.H. Chu, L.W. Martin, M.B. Holcomb, Q. He, P. Maksymovych, N. Balke, S.V. Kalinin, A.P. Baddorf, S.R. Basu, M.L. Scullin, R. Ramesh, Electric modulation of conduction in multiferroic Ca-doped BiFeO3 films, Nat. Mater. 8 (2009) 485–493. https://doi.org/10.1038/nmat2432.
29. M. Li, F. Zhuge, X. Zhu, K. Yin, J. Wang, Y. Liu, C. He, B. Chen, R.-W. Li, Nonvolatile resistive switching in metal/La-doped BiFeO 3 /Pt sandwiches, Nanotechnology. 21 (2010) 425202. https://doi.org/10.1088/0957-4484/21/42/425202.
30. A. Lahmar, S. Habouti, M. Dietze, C.-H. Solterbeck, M. Es-Souni, Effects of rare earth manganites on structural, ferroelectric, and magnetic properties of BiFeO 3 thin films, Appl. Phys. Lett. 94 (2009) 012903.
31. A. Lahmar, S. Habouti, C.-H. Solterbeck, M. Es-Souni, B. Elouadi, Correlation between structure, dielectric, and ferroelectric properties in BiFeO3–LaMnO3 solid solution thin films, J. Appl. Phys. 105 (2009) 014111. https://doi.org/10.1063/1.3063813.
32. L. Liu, S. Zhang, Y. Luo, G. Yuan, J. Liu, J. Yin, Z. Liu, Coexistence of unipolar and bipolar resistive switching in BiFeO3 and Bi0.8Ca0.2FeO3 films, J. Appl. Phys. 111 (2012) 104103. https://doi.org/10.1063/1.4716867.
33. D.S. Jeong, R. Thomas, R.S. Katiyar, J.F. Scott, H. Kohlstedt, A. Petraru, C.S. Hwang, Emerging memories: resistive switching mechanisms and current status, Rep. Prog. Phys. 75 (2012) 076502. https://doi.org/10.1088/0034-4885/75/7/076502.
34. D. Rubi, F.G. Marlasca, M. Reinoso, P. Bonville, P. Levy, Magnetism and electrode dependant resistive switching in Ca-doped ceramic bismuth ferrite, Mater. Sci. Eng. B. 177 (2012) 471–475. https://doi.org/10.1016/j.mseb.2012.02.022.
35. J.M. Luo, S.P. Lin, Y. Zheng, B. Wang, Nonpolar resistive switching in Mn-doped BiFeO3 thin films by chemical solution deposition, Appl. Phys. Lett. 101 (2012) 062902. https://doi.org/10.1063/1.4742897.
36. G. Kartopu, A. Lahmar, S. Habouti, C.-L. Solterbeck, B. Elouadi, M. Es-Souni, Observation of structural transitions and Jahn–Teller distortion in LaMnO3-doped BiFeO3 thin films, Appl. Phys. Lett. 92 (2008) 151910. https://doi.org/10.1063/1.2903490.
37. A. Lahmar, M. Es-Souni, Sequence of structural transitions in BiFeO3–RMnO3 thin films (R=Rare earth), Ceram. Int. 41 (2015) 5721–5726. https://doi.org/10.1016/j.ceramint.2014.12.157.
38. A.N. Ulyanov, D.-S. Yang, S.V. Savilov, Negative magnetization, shielding current effect and divalent manganese in CaMn1-Ta O3 manganites, J. Alloys Compd. 967 (2023) 171686. https://doi.org/10.1016/j.jallcom.2023.171686.
39. R. Bharamagoudar, V.J. Angadi, I. Shivaraja, B. Angadi, R. Mondal, A.S. Patil, S. Patil, V. Pattar, S. Raghu, S. Matteppanavar, Evidence of Weak Ferromagnetism, Space Charge Polarization, and Metal to Insulator Transition in Dy-Doped CaMnO3, J. Supercond. Nov. Magn. 34 (2021) 837–844. https://doi.org/10.1007/s10948-020-05770-1.
40. R. Bharamagoudar, S. Matteppanavar, A.S. Patil, V. Pattar, J.A. V, K. Manjunatha, Effect of Dy on structural and low temperature magnetic properties of Ca0.7Dy0.3MnO3, Chem. Data Collect. 24 (2019) 100288. https://doi.org/10.1016/j.cdc.2019.100288.
41. J.B. MacChesney, H.J. Williams, J.F. Potter, R.C. Sherwood, Magnetic Study of the Manganate Phases: CaMnO3, Ca4Mn3 O10, Ca3Mn2O7, Ca2MnO4, Phys. Rev. 164 (1967) 779–785. https://doi.org/10.1103/PhysRev.164.779.
42. P.W. Anderson, New Approach to the Theory of Superexchange Interactions, Phys. Rev. 115 (1959) 2–13. https://doi.org/10.1103/PhysRev.115.2.
43. Z. Zeng, M. Greenblatt, M. Croft, Large magnetoresistance in antiferromagnetic CaMnO3 − δ, Phys. Rev. B. 59 (1999) 8784–8788. https://doi.org/10.1103/PhysRevB.59.8784.
44. A. Lahmar, Multiferroic properties and frequency dependent coercive field in BiFeO3 -LaMn0.5Co0.5O3 thin films, J. Magn. Magn. Mater. 439 (2017) 30–37. https://doi.org/10.1016/j.jmmm.2017.04.096.
45. F. Yan, T.J. Zhu, M.O. Lai, L. Lu, Enhanced multiferroic properties and domain structure of La-doped BiFeO3 thin films, Scr. Mater. 63 (2010) 780–783. https://doi.org/10.1016/j.scriptamat.2010.06.013.

46. B. Zhao, Z. Chen, J. Meng, H. Lu, D.W. Zhang, A. Jiang, Ferroelectric polarization and defect-dipole switching in an epitaxial (111) BiFeO3 thin film, J. Appl. Phys. 117 (2015) 204103. https://doi.org/10.1063/1.4921808.
47. C.M. Folkman, S.H. Baek, C.T. Nelson, H.W. Jang, T. Tybell, X.Q. Pan, C.B. Eom, Study of defect-dipoles in an epitaxial ferroelectric thin film, Appl. Phys. Lett. 96 (2010) 052903. https://doi.org/10.1063/1.3298362.
48. B. Xu, C. Paillard, B. Dkhil, L. Bellaiche, Pinched hysteresis loop in defect-free ferroelectric materials, Phys. Rev. B. 94 (2016) 140101. https://doi.org/10.1103/PhysRevB.94.140101.
49. T. Choi, S. Lee, Y.J. Choi, V. Kiryukhin, S.-W. Cheong, Switchable Ferroelectric Diode and Photovoltaic Effect in BiFeO3, Science. 324 (2009) 63–66. https://doi.org/10.1126/science.1168636.
50. D. Lee, S.H. Baek, T.H. Kim, J.-G. Yoon, C.M. Folkman, C.B. Eom, T.W. Noh, Polarity control of carrier injection at ferroelectric/metal interfaces for electrically switchable diode and photovoltaic effects, Phys. Rev. B. 84 (2011) 125305. https://doi.org/10.1103/PhysRevB.84.125305.
51. R. Waser, M. Aono, Nanoionics-based resistive switching memories, Nat. Mater. 6 (2007) 833–840.
52. R. Waser, R. Dittmann, G. Staikov, K. Szot, Redox-Based Resistive Switching Memories - Nanoionic Mechanisms, Prospects, and Challenges, Adv. Mater. 21 (2009) 2632–2663. https://doi.org/10.1002/adma.200900375.